The Impact of Dynamic Viscosity of Glycerin Solutions on a Submerged Oscillating Mass-Spring System

How does the dynamic viscosity of aqueous glycerin solutions affect the damping force applied to a submerged oscillating mass-spring system?

IB Physics

Word Count: 3969

Contents

Introduction

Simple harmonic motion (SHM) describes the motion of an object oscillating indefinitely, for example, an oscillating mass suspended by springs. Damped oscillation is similar to SHM, except the oscillating object is damped by some external force, thereby gradually returning to its equilibrium position (Taylor 173). When the damping force is caused by a liquid, it is referred to as a viscous drag force, and its magnitude depends on the liquid's viscosity (Munson et al 377).

Glycerin is a liquid substance that dissolves in water and its solution's viscosity changes as glycerin concentration changes. We created a damped-oscillation system with variable viscosity if we submerge a mass-spring system under glycerin solutions. This begs the following research question: how does the dynamic viscosity of aqueous glycerin solutions affect the damping force applied to a submerged oscillating mass-spring system?

We aimed to predict the behavior of the system and compared it with the experimental results. Before conducting the main experiment, we first did two mini-experiments to measure some unknowns: the dynamic viscosity of glycerin solution at various concentrations (the independent variable) and the effective spring constant of the springs in the system (a control variable).

Part I: Measuring the Viscosity of Glycerin Solutions

We measured the dynamic viscosity of aqueous glycerin solutions using a self-built capillary viscometer and compared the measurements to some published values.

Background

Viscosity quantitatively measures the fluid resistance to flow, by determining the fluid strain rate generated by applied shear stress (White 25), where shear stress is the force causing the

fluid to flow and the strain rate is the rate of shape change in the fluid over time (Munson et al 16-17).

Fluids can be divided into two main categories: Newtonian and non-Newtonian fluids. All Newtonian fluids' shear stress is linearly proportional to their strain rate (Munson et al 15). There are two metrics of viscosity. If we plot the strain rate against shear stress, the slope of the line represents dynamic viscosity (Munson et al 15). We can also find the kinematic viscosity of a fluid by dividing the dynamic viscosity by fluid density.

Since aqueous glycerin solutions are Newtonian fluids, we can measure their viscosity using a capillary viscometer, as shown in Fig. 1.

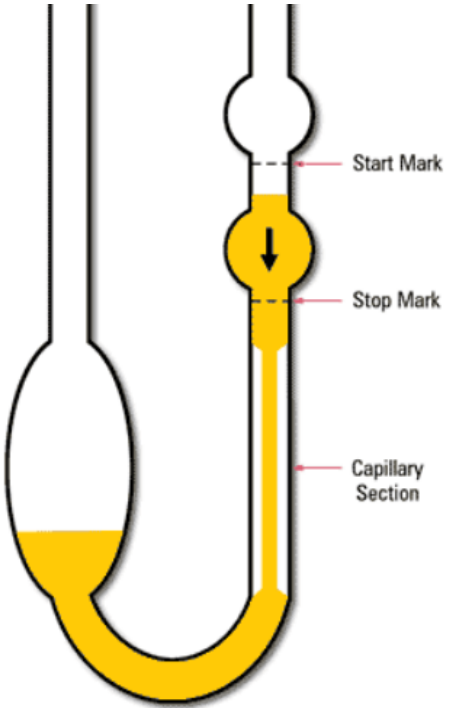

Figure 1: Example Geometry of a capillary viscometer (Troyer).

Eq. 1 below characterizes the dynamic viscosity measured using a capillary viscometer, where k_v is the calibration constant, determined by calibrating the viscometer, η is the dynamic

viscosity, t_v is the time taken for a fluid to flow from the start mark to the stop mark, and ρ is the fluid density ("2.2.9. Capillary Viscometer").

$$\eta = k_v \rho t_v \tag{1}$$

This equation is later used to calculate the experimental dynamic viscosity of glycerin solutions.

Methodology

We built a simplified viscometer by gluing a 1" acrylic tube to an acrylic plate with a 5/32" opening, then used a 150mL beaker to collect the liquid, as shown in Fig. 2 below.

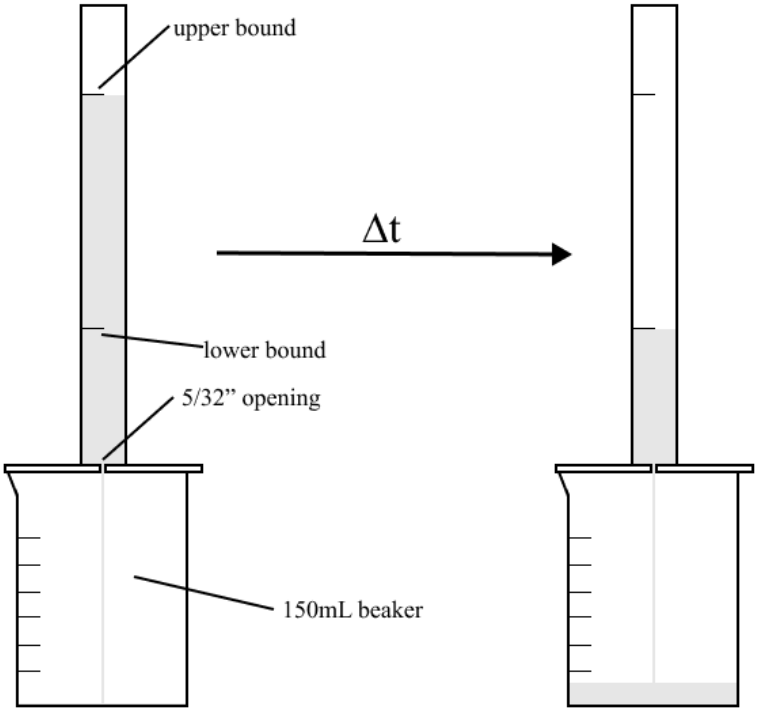

Figure 2: The apparatus for calibrating the viscometer.

The upper bound and the lower bound each correspond to the start and stop mark labeled in Fig. 1. We filled the tube with liquids and recorded the fluid level dropping at 30 frames per second (FPS).

In Eq. 1, there are three variables needed to calculate the dynamic viscosity: the calibration constant, the fluid density, and the flowtime. We calculated the density of glycerin solutions by weighing a sample of pure glycerin and finding the weighted average of the density of water and glycerin, as shown by the equation below.

$$\rho = \rho_w C_w + \rho_g C_g \tag{2}$$

The subscript "*w"* denotes variables associated with water, and "*g"* is associated with pure glycerin. The variable *C* indicates its concentration by volume.

We also found the flowtime by counting the number of frames passed as the fluid level dropped from the upper to the lower bound and divided it by the framerate.

Finding the calibration constant required us to calibrate the viscometer. We chose motor oils as calibration fluids due to ease of access. We obtained their standardized viscosity indices at different temperatures from the websites of major lubricant manufacturers and regulators ("Graph Your Oils"; "Viscosity Indices"). Their flowtimes were measured and plotted against their kinematic viscosity, and the slope of the linear best-fit line represents the calibration constant.

We then calculated the viscosity of glycerin solutions and cross-referenced them with other literature. Five trials were recorded and processed for each calibration fluid and concentration of glycerin solution, with an additional trial recorded for each concentration in case a trial contained blurry footage. Since temperature can impact viscosity, in addition to experimenting in a lab with climate controls, a temperature reading of the lab was also recorded periodically.

Results

The recorded temperature inside the lab was consistent throughout the experiment, at 22°C. Due to the lack of database viscosity values for motor oils at 22°C, we plotted the kinematic

viscosity of various oils against temperature, and their viscosity index was interpolated via two methods. We chose to average the result from two methods to minimize random error. The first method is manually fitting a transformed $\frac{1}{x}$ function using the equation below as the base function.

$$\upsilon_{fit} = \frac{a}{x-b} + c$$

The $\frac{1}{x}$ function is chosen because the viscosity of a liquid grows asymptotically as the temperature approaches its freezing point and asymptotes to 0 as the temperature becomes infinitely large. This description best fitted a transformed $y = \frac{1}{x}$ function.

The second method is to model the viscosity trend as a piecewise function, by assuming the change in viscosity between the two adjacent temperatures is linear. Since 5°C and 10°C steps are quite small compared to the operating temperature range of motor oils, a piecewise interpolation is quite accurate. A line that crosses the two closest data points is used to interpolate the oil viscosity at 22°C. Fig. 3 below shows an example interpolation of oil viscosity at 22°C.

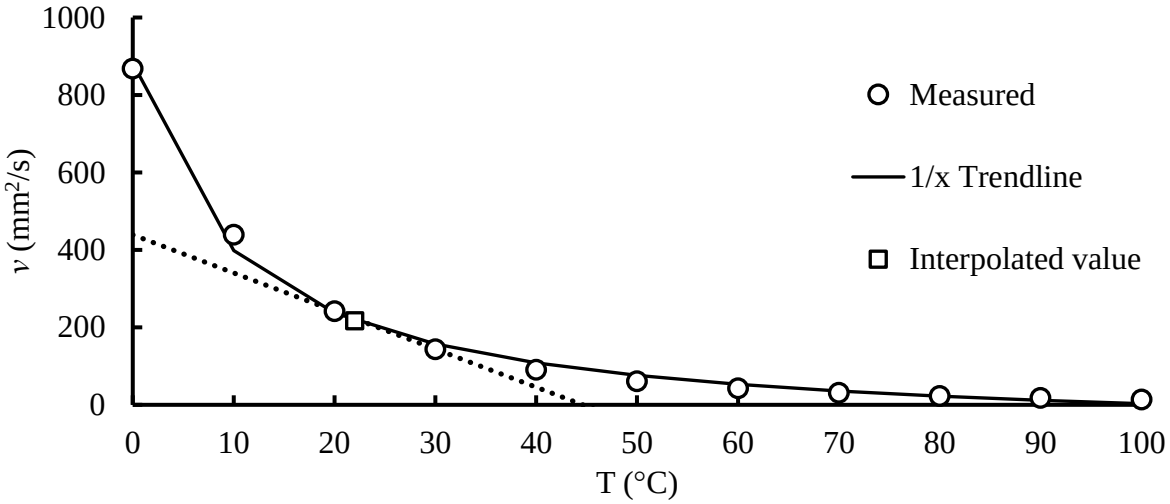

Figure 3: Interpolation for the kinematic viscosity of 5W-40 motor oil at 22°C.

The resultant kinematic viscosity indices, υ_{fit} and $\upsilon_{piecewise}$, were then averaged and divided by the average flowtime of their corresponding fluids to obtain the calibration constant.

Table 1 below shows that each calibration fluid produced a different calibration constant. This suggests that the calibration of the viscometer is invalid because the calibration constant should not change drastically.

Table 1: Measurements produced by calibrating of the viscometer.

Material	**Ave. Flowtime** (s ± 0.004 s)	$\boldsymbol{v}_{fit}$ (mm^2/s)	$\boldsymbol{v}_{piecewise}$ (mm^2/s)	$\boldsymbol{v}_{ave}$ (mm^2/s)	$\boldsymbol{k}_v$ (mm^2/s^2)	$\boldsymbol{k}_{v\,ave}$ (mm^2/s^2)
Water	3.407	0.957			0.281	9.2
5W-40	17.760	217.19	222.42	220 ± 3	12.4	
0W-20	9.313	102.84	105.52	104 ± 2	11.2	
75W-140	39.187	436.68	440.98	439 ± 2	11.2	
ATF	6.820	71.964	75.152	74 ± 2	11	

Since capillary viscometers are only calibrated to accurately measure a small range of fluid viscosities by assuming the increase in kinematic viscosity is linear ("2.2.9. Capillary Viscometer"), fluids with very different viscosity indices will not produce a consistent calibration constant. This is because the increase in viscosity, in reality, is non-linear.

Nonetheless, we decided to derive the viscosity of glycerin solutions using the viscometer and compared the results to previous literature. We measured the mass of a 10mL sample of glycerin and found its density: 1.262 ± 0.001 g/cm^3. The densities of glycerin solutions were then calculated using the following equation, assuming the density of water is 1.000 ± 0.001 g/cm^3.

$$\rho = \rho_w C_w + \rho_g C_g \tag{2}$$

The η_{calc}, the calculated viscosity, is based on a python algorithm written by Dr. Matthew Partridge at Cranfield University ("Calculate Density"). This algorithm calculates the dynamic viscosity of glycerin solutions by combining the Andrea Volk Polynomial Method to model the density of glycerin solutions at different concentrations and temperatures (Volks and Kähler), and

the empirical formula proposed by Cheng to approximate the kinematic viscosity of glycerin solutions (Cheng).

Both Table 2 and Fig. 4 below show that the experimentally determined viscosity is very different from the calculated values. This corroborates with the theory that the viscosity reading produced by this viscometer is inaccurate due to the lack of consistency of its calibration constant.

Table 2: Experimentally derived viscosity of glycerin solutions.

Concentration by Volume (%)	**Ave. Flowtime** (s ± 0.004 s)	$\boldsymbol{\upsilon}_{\boldsymbol{exp}}$ $(mm^2/s \pm 1\ mm^2/s)$	$\boldsymbol{\rho}_{\boldsymbol{exp}}$ $(mg/mm^3 \pm 0.001\ mg/mm^3)$	$\boldsymbol{\eta}_{\boldsymbol{exp}}$ $(mPa \cdot s \pm 1\ mPa \cdot s)$	$\boldsymbol{\eta}_{\boldsymbol{calc}}$ $(mPa \cdot s)$
80	6.933	64	1.210	77	80.347
70	4.453	41	1.183	48	31.470
60	4.013	37	1.157	43	14.618
50	3.613	33	1.131	37	7.711
40	3.567	33	1.105	36	4.484
30	3.507	32	1.079	35	2.814
20	3.513	32	1.052	34	1.876
10	3.447	32	1.026	32	1.314

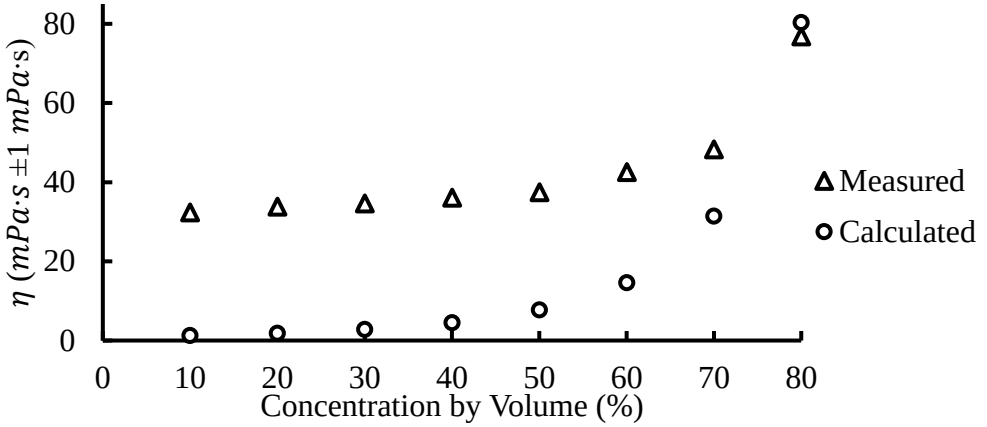

Figure 4: Comparison between the measured and theoretical dynamic viscosity of glycerin solutions.

Even though the different sources of the glycerin can have different viscosity, it cannot account for the huge difference shown in Fig. 4. The error bars are also tiny (blocked by the points in the graph), suggesting random error is not responsible for the large discrepancy. Therefore, since

the viscometer failed to produce reasonable measurements, the rest of the experiment used the viscosity calculated by the aforementioned python algorithm.

Part II: Determining the Spring Constant

We did a Hooke's law experiment to determine the spring constant.

Methodology

Fig. 5 below shows the apparatus used to determine the spring constant. According to Hooke's law, when a mass is attached to a spring vertically, the extension of the spring is proportional to $-\frac{g}{k}$, as shown in Eq. 3.

$$\begin{aligned} mg &= kx \\ x &= \frac{g}{k}m \end{aligned} \tag{3}$$

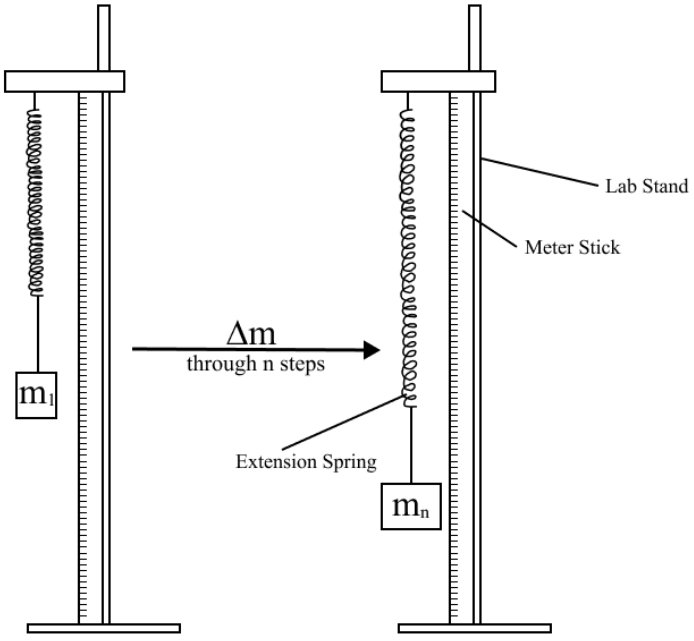

Figure 5: The apparatus of Hooke's law experiment.

After attaching lab weights to the spring, the displacement of the leading edge of the extension spring was measured using the meterstick shown in Fig. 5.

Results

After taking five sets of measurements, the displacement of the spring is calculated and averaged across the sets. The average displacement is then plotted against the total mass of the attached lab weights, as shown in Fig. 6 below.

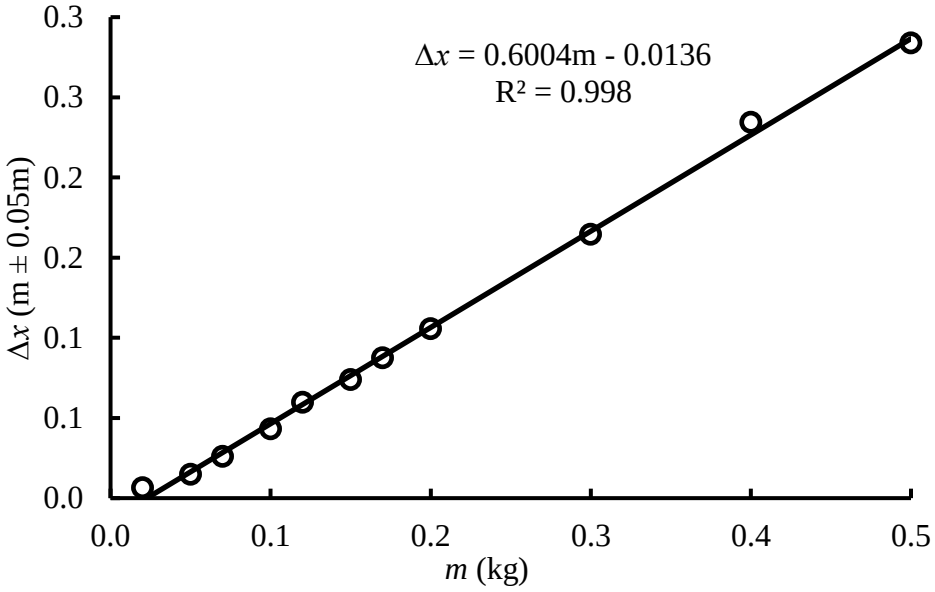

Figure 6: Position of the leading edge of the chain of extension springs versus the total mass of the attached lab weights.

As shown in Eq. 3, the slope of the equation, 0.6004, represents $\frac{g}{k}$, where $g = 9.81\ m\ s^{-2}$. We find that k, the effective spring constant, is 16.3 N m^{-1}. The best fit line has an R^2 value of 0.998, indicating a very strong linear relationship with few uncertainties. The vertical error bars are tiny (blocked by the points in the graph). Hence, even without the propagated uncertainties, we considered the derived spring constant a reliable value.

Part III: Main Experiment

Theory

The main experiment aims to determine whether the viscosity of the glycerin solution affects the damping strength experienced by a submerged sphere suspended by springs. Fig. 7 below shows the free-body diagram (FBD) of the apparatus.

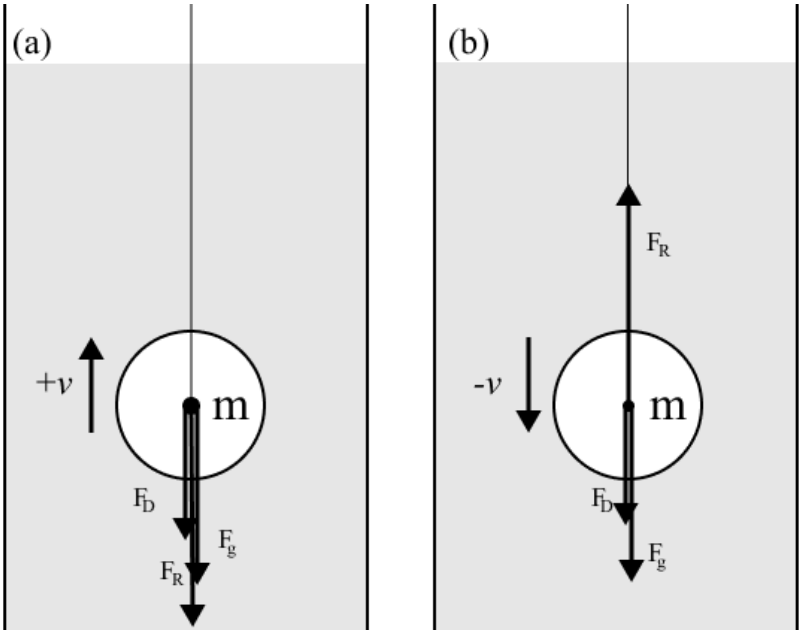

Figure 7: FBDof the forces acting on the spherical mass oscillating in the column of fluid.

Three significant forces are acting on the sphere: the spring restoring force (F_R), the gravitational force (F_g), and the drag force (F_D). A buoyancy force is also present but insignificant since lead is much denser than glycerin. We can express the FBD using the following equation:

$$F_{net} = F_R - F_D - F_g$$

$$ma = -kx - \alpha v - mg$$

We define m as the mass of the sphere, k as the effective spring constant, and α as the damping constant, proportional to the drag force. The drag force can be predicted using Stokes'

Law, an experimentally determined law that characterizes the drag force experienced by a submerged, slowly moving sphere, shown in the equation below. (Fowler).

$$F_D = 6\pi\eta R v$$

R and v each represent the radius and the velocity of the sphere. Since $F_D = \alpha v$, we find:

$$\alpha = 6\pi\eta R$$

Rearranging the Newton's second law equation by rewriting the acceleration, *a*, as the second derivative of *x*, the vertical position, and *v*, the velocity, as the first derivative of *x*, we get:

$$\frac{d^2x}{dt^2} = -\frac{k}{m}x - \frac{\alpha}{m}\frac{dx}{dt}$$

Note the gravitational force is not in the differential equation because the derivative of a constant is 0. To solve this equation, we need the equation below:

$$x(t) = A_0 e^{bt}\cos\omega t$$

This is the general equation for damped oscillation, where A_0 is the initial amplitude, b is related to the damping constant, and ω is the angular frequency. By differentiating this equation, we get:

$$\frac{dx}{dt} = A_0(be^{bt}\cos\omega t - \omega e^{bt}\sin\omega t)$$
$$\frac{d^2x}{dt^2} = A_0[(b^2-\omega^2)(e^{bt}\cos\omega t) - 2\omega b(e^{bt}\sin\omega t)]$$

After substituting the derivatives into the differential equation and factoring out common factors, we get:

$$(b^2-\omega^2)(e^{bt}\cos\omega t) - 2\omega b(e^{bt}\sin\omega t) = -\frac{k}{m}(e^{bt}\cos\omega t) - \frac{\alpha}{m}(be^{bt}\cos\omega t - \omega e^{bt}\sin\omega t)$$

Since there is at least a term on each side that contains a $\sin\omega t$ and a $\cos\omega t$, we can conclude that the sum of all terms on the left-hand side with a $\sin\omega t$ must equal the sum of all

terms on the right-hand side with a $\sin \omega t$, and vice versa with $\cos \omega t$. Therefore, we can split the equation above into the following equations by isolating the terms with $\sin \omega t$ and a $\cos \omega t$. We get the following two equations:

$$(b^2-\omega^2)(e^{bt}\cos \omega t) = -\frac{(k+\alpha b)(e^{bt}\cos \omega t)}{m} \quad (3)$$

and

$$2mb\omega e^{bt}\sin \omega t = -\alpha\omega e^{bt}\sin \omega t$$
$$b = -\frac{\alpha}{2m}$$

After substituting $-\frac{\alpha}{2m}$ into Eq. 3 and isolating ω, it simplifies to:

$$\omega = \frac{\sqrt{4km-\alpha^2}}{2m}$$

We substituted ω and b back into the general equation and found Eq. 4 below:

$$x(t) = A_0 e^{-\frac{\alpha t}{2m}}\cos\left(\frac{\sqrt{4km-\alpha^2}}{2m}t\right) \quad (4)$$

Eq. 4 summarizes the theoretical model of the submerged sphere's motion. We used it to predict the vertical position of the sphere and compared it to the measured positions.

Methodology

We aim to experimentally determine the impact of the viscosity of glycerin solutions on the motion of a submerged sphere. Fig. 8 below shows the experimental apparatus for measuring the vertical position of the sphere.

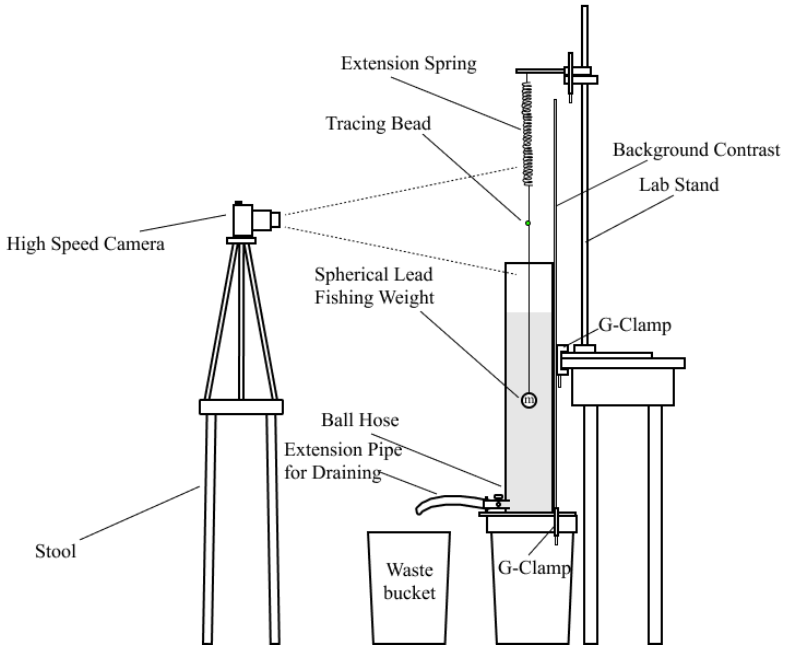

Figure 8: The apparatus of the main experiment.

A lead sphere (44mm in diameter) is suspended via a chain of extension springs with a spring constant of 16.3 N m^{-1} and a thin, non-stretchable steel cable. A tracing bead is also attached to the cable. The sphere was dropped into a vertical, cylindrical column of aqueous glycerin solutions of various concentrations (all concentrations are measured by volume), with a diameter of 5.75 inches. We chose to use a tube with a large internal diameter to minimize boundary layer and eddie frictions, which are other potential damping forces associated with a fluid-solid system (White). A high-speed camera recorded the movement of the tracing bead at 240 frames per second (FPS). We then tracked the movements using a video analysis software called Tracker. Due to the camera's limitations, it was only able to record roughly 6 seconds of useful footage.

The range of concentrations of aqueous glycerin solutions used in this experiment starts at 80%, reduced by 10% per step. We diluted and stirred the solution until no separation between water and glycerin is visible. We also measured the oscillation of the sphere in water and air as

baseline trials. Fig. 9 below shows the setup of Tracker and the features used to obtain the vertical positions of the sphere.

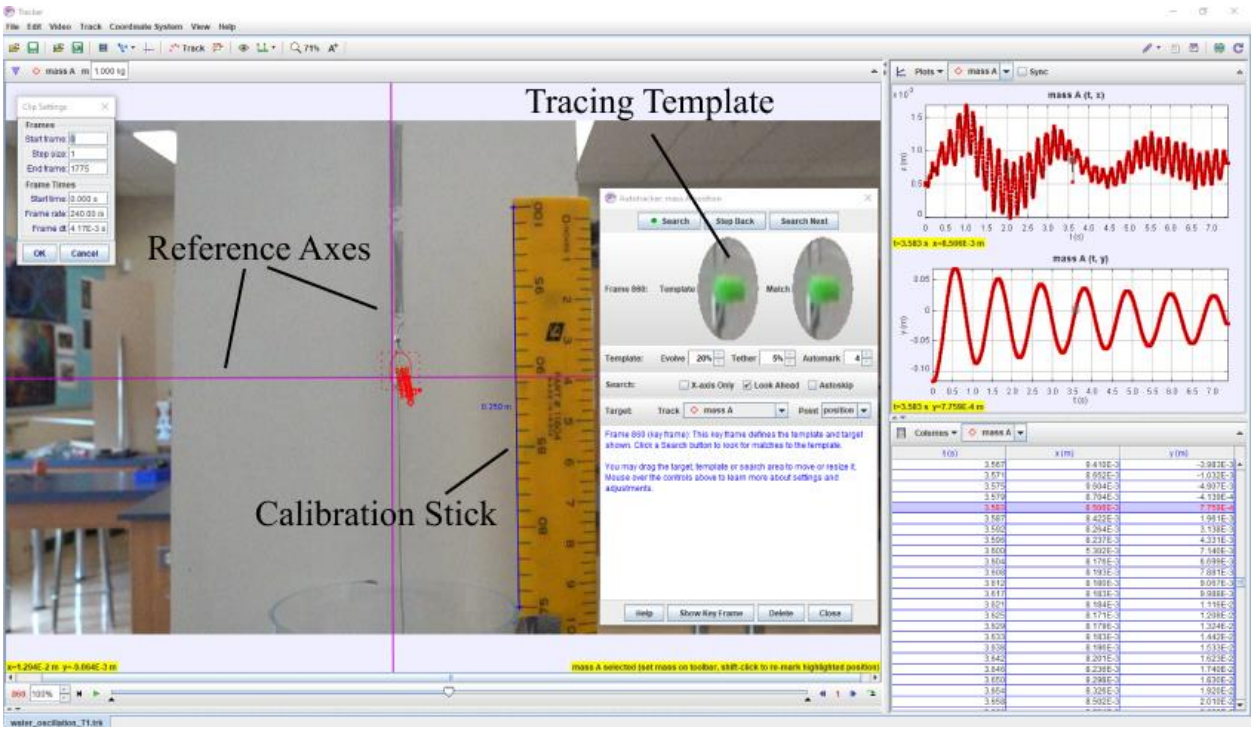

Figure 9: Screenshot of Tracker processing the movements of the lead sphere for trial 1 of 0% glycerin (water).

The calibration stick, or the blue line next to the yellow meterstick, adds a scale to the images using the graduations on the meterstick. The purple lines represent the axes, and the y-axis is parallel to the calibration stick. Since the horizontal position of the sphere is insignificant in this experiment, it remains uncalibrated. The tracing bead is used as a template for tracking and the auto-tracker records the coordinate of the collection of pixels closest to the template. The frame rate of the video is set to 240 FPS. Tracker assigned a timestamp to every processed frame.

We corrected the measured positions such that all trials for each glycerin concentration have the same maximum amplitude and have no vertical offset. We vertically shifted them up by

0.007m, then stretched or compressed them vertically such that their maximum amplitude is 0.1m. We also phase-shifted the measured positions such that the first peak is at $t = 0$.

Then, the measured positions across the multiple trials were averaged, and the theoretical vertical position of the sphere is compared to the measured positions graphically. The theoretical positions were calculated using Eq. 4 below:

$$x(t) = A_0 e^{-\frac{\alpha t}{2m}} \cos\left(\frac{\sqrt{4km-\alpha^2}}{2m} t\right) \quad (4)$$

Results

As shown in Fig. 10 below, the measured vertical positions of the sphere (referred to as "measured positions" from here on) submerged under glycerin solutions all showed some damping, whereas the sphere oscillating in air showed no damping.

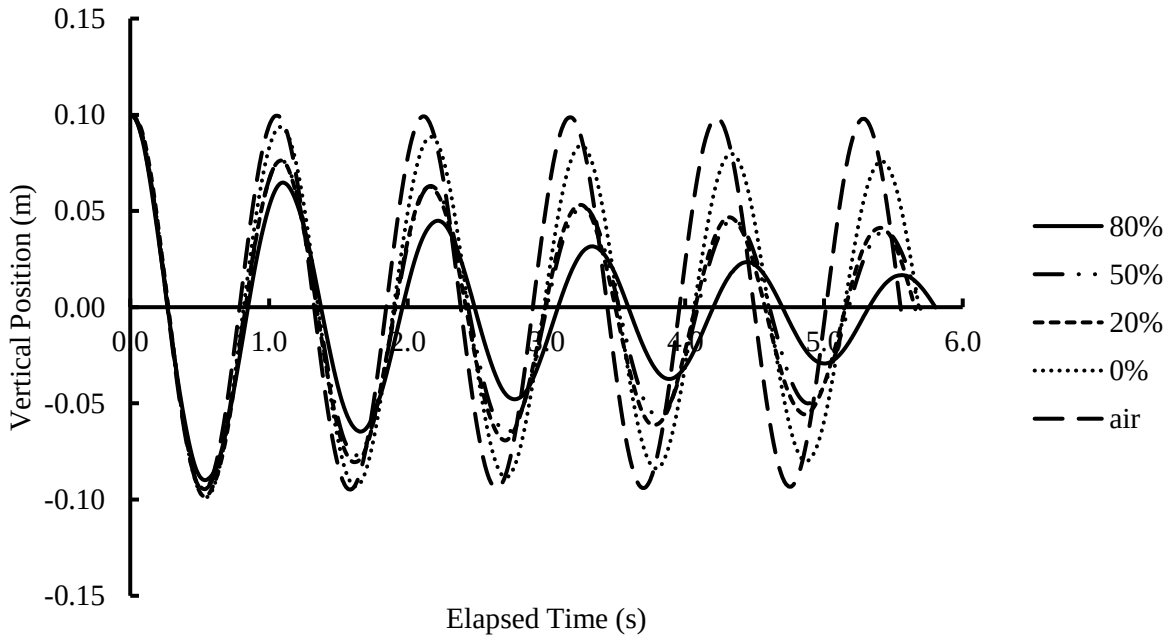

Figure 10: Comparison of the average vertical position of the lead sphere versus elapsed time across multiple concentrations.

Fig. 11 below shows that the theoretical and measured positions do not match.

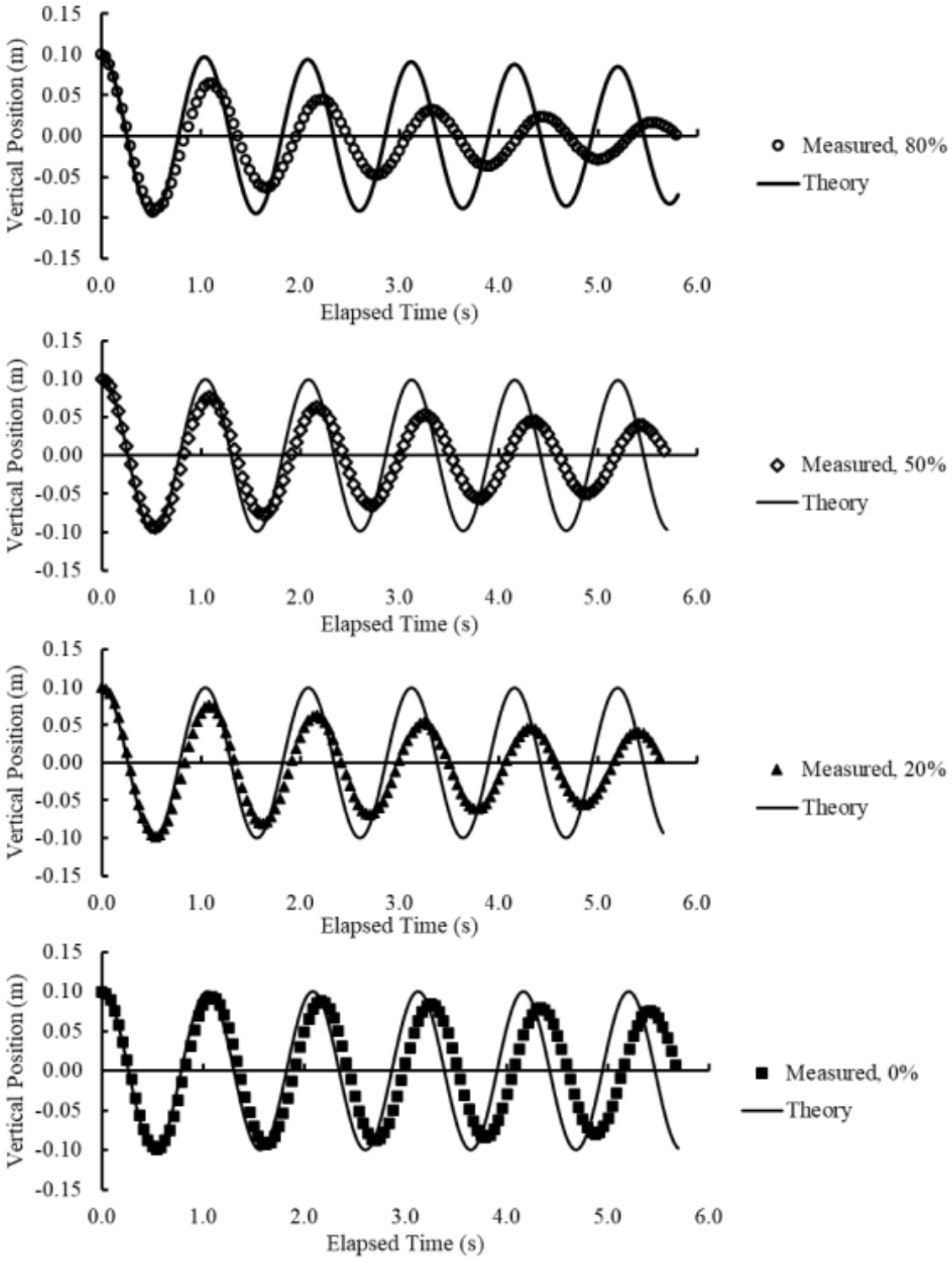

Figure 11: Comparison between the theoretical and measured position of the lead sphere in various glycerin solutions.

There are two major discrepancies between the theory and the measured positions: the damping force experienced by the sphere and the period of oscillation.

Strength of Damping

We first assessed why the measured positions showed stronger-than-predicted damping. To avoid confirmation bias, we re-examined the measured positions while ignoring the theory. One interesting trend emerged after comparing the strength of damping when submerged under water and glycerin solutions, as shown in Fig. 12 below.

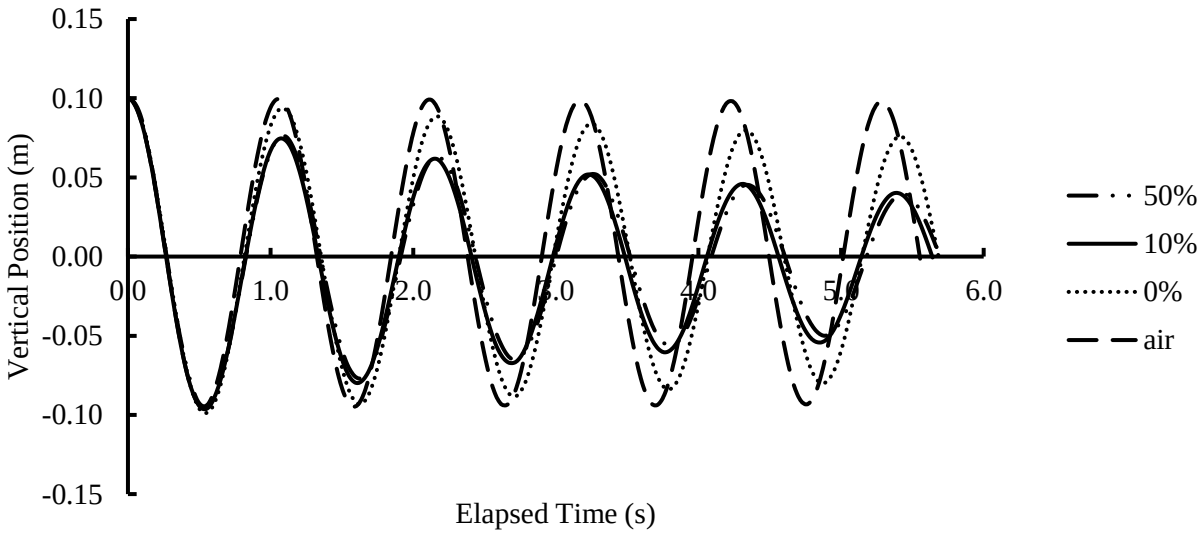

Figure 12: Comparison of the average vertical position when submerged in 10%, 50%, and 0% glycerin solutions.

Due to their low viscosity, the measured position in air showed no significant damping, and only lightly damped in water. Interestingly, when submerged in 20% or 50% glycerin solutions, the sphere experience similar strength of damping. The difference in damping strength in water and the 20% glycerin, however, is quite large. This is strange because the 50% glycerin solutions are much more viscous than 20% glycerin, and 20% glycerin is only fractionally more viscous than water. This disagrees with the theory, suggesting viscosity may not be the only factor affecting the strength of damping.

Two potential reasons could account for this phenomenon. The first possibility is that the drag experienced by the sphere is not linear, but quadratic. Stokes' Law, the relationship used to predict the damping strength, can only accurately approximate the drag force exerted by the fluid given the sphere is slowly moving through the fluid, meaning the flow is assumed to be laminar (Fowler). However, the oscillation may have caused some turbulence, and affected the accuracy of the approximation.

To check this theory, several sample Reynolds number calculations were performed. Reynolds number (Re) is the ratio between inertial and viscous forces in a fluid, which can help indicate if the flow is turbulent (White 27). To approximate the Reynolds number of the mass-spring system, we changed the frame of reference. We perceived and analyzed the sphere, the moving object in a stationary system, as a stationary object in a moving system. Therefore, the Reynolds number of the mass-spring system can be approximated using the equation below, where d represents the diameter and v represents the velocity of the sphere (Urone 503).

$$Re = \frac{\rho v d}{\eta} = \frac{6mvr^4}{4\pi}$$

Table 3: Average and maximum Reynolds number of each glycerin concentration.

Conc.	**80%**	**70%**	**60%**	**50%**	**40%**	**30%**	**20%**	**10%**	**0%**
Re_{ave}	1040	3240	7420	14800	27600	43500	63500	89300	149000
Re_{max}	3350	9150	19300	37000	68200	105000	159000	219000	290000

Considering transition flow occurs when the Reynolds number is between 1000 and 2000, and all fluid flows are turbulent when the Reynolds number exceeds 2000 (Urone 504), Table 3 suggests that for all concentrations, the oscillation likely caused some turbulence. In addition, the rough surface of the sphere is likely to cause additional turbulence in fluid flow. Therefore, evidence indicates that Stokes' Law is inaccurate at approximating the drag force in this case.

Instead, the general drag formula, where the drag force increases quadratically as the velocity increases, may be a better method for approximating the damping force experienced by the sphere. The equation below is the general drag formula, where Cd is the coefficient of drag, ρ is the density of the fluid, and A is the largest cross-sectional area of the sphere.

$$F_D = Cd\frac{\rho A v^2}{2}$$

To calculate the drag force experienced by the sphere using this formula, the drag coefficient must be obtained. One possible method uses the system's Reynolds number and approximates the drag coefficient through a pre-determined function; but it is only accurate for low Reynolds numbers, which makes it unsuitable in this case (Mikhailov and Freire 433). Another method uses a physical or computationally simulated wind tunnel to measure the drag force under various flow conditions. However, we have no access to wind tunnels, and simulating the drag force through a computational-fluid dynamics software is also unsuitable due to the geometry of the sphere consisting of many rough surfaces that are hard to model computationally. Therefore, confirming if the drag experienced by the sphere can be characterized by the general drag formula is out of the scope of this investigation.

The second theory to account for the stronger-than-predicted damping is that the drag force experienced by the sphere is not solely related to the viscosity of the fluids, but also the presence of glycerin.

Although categorized as a Newtonian fluid, aqueous solutions of glycerin behave strangely with water (Rehm et al). Glycerin modifies the hydrogen bond networks in water, which changes the physical properties of their solutions (Towey and Dougan). Therefore, it suggests the presence of glycerin in the solution alone could have a significant effect on damping the oscillation.

However, modeling and verifying this behavior requires extensive analysis of the chemical properties of glycerin, which is also beyond the scope of this investigation.

Since the theoretical and the measured positions disagree, we tried to experimentally determine the relationship between viscosity and the strength of damping experienced by the sphere.

The damping constant, α, was manually derived for each concentration, by plotting the peak of each period against elapsed time. The equation below represents both the relationship between α and the measured positions and the exponential decay envelope of the maximum amplitude:

$$x = 0.1e^{-at}$$

We then plotted the damping constants against their dynamic viscosity, in Fig. 13 below.

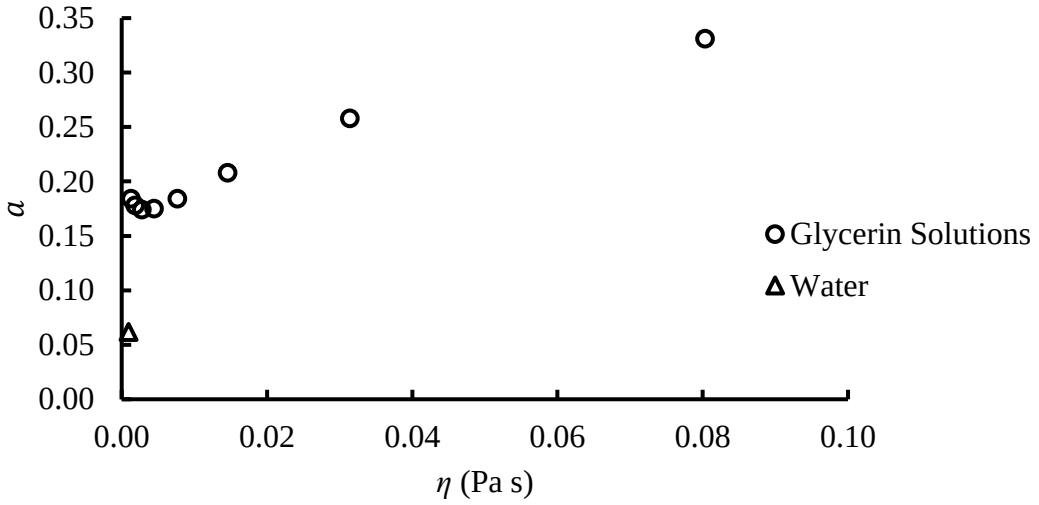

Figure 13: The relationship between the damping constant and dynamic viscosity.

We see the damping constant increases as the dynamic viscosity increases. The damping constant in water is significantly lower than in other concentrations, which would support that the presence of glycerin increases the strength of the damping. This relationship seems somewhat

linear, but the clustering of data at low viscosity indicates alternative possibilities. We then plotted α, the damping constant, against C, the concentration of glycerin, as shown in Fig. 14 below.

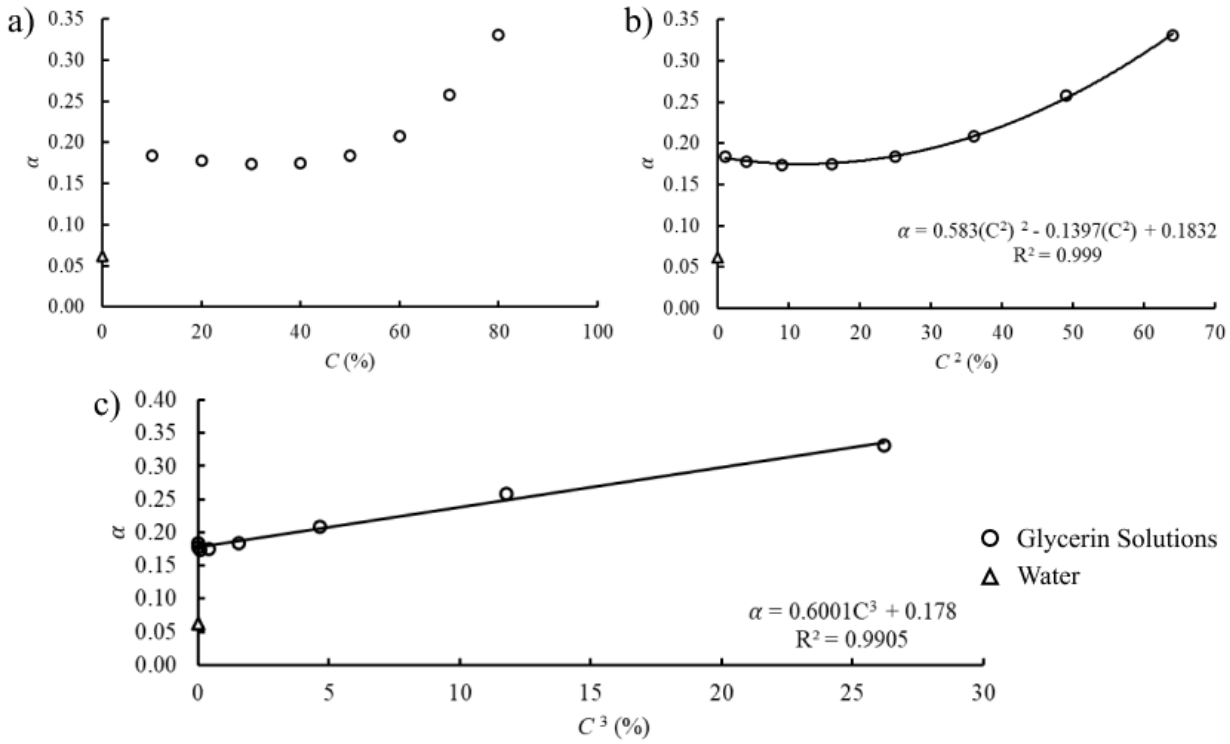

Figure 14: the relationship between the damping constant and glycerin concentration.

Fig. 14a and 14b show a non-linear, and possibly quartic relationship between concentration and the damping constant. We tried to linearize the relationship by cubing the concentration and taking the concentration to the fourth power.

The R^2 value for both concentrations cubed (Fig. 14c) and taking the concentration to the fourth power (Fig. 15 below) are both quite high, with concentrations cubed being slightly higher. This is interesting because neither the theory nor any previous literature suggested a cubic or a quartic relationship between concentration and the damping constant.

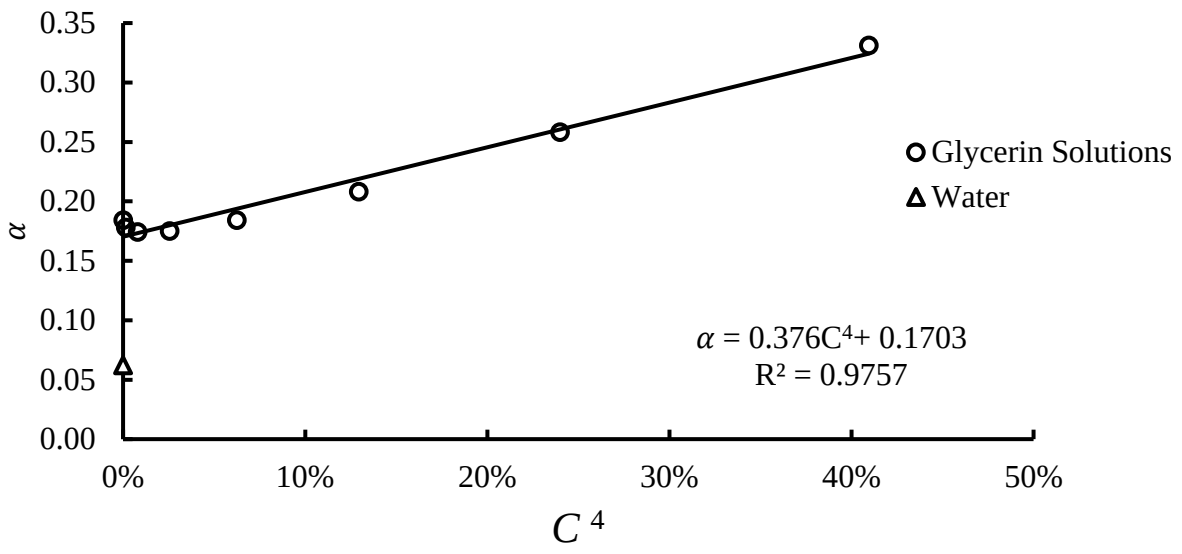

Figure 15: The relationship between the damping constant and the concentration of glycerin taken to the fourth power.

Period of Oscillation

We also explored why the theoretical and the measured periods do not agree. The periods are related to the damping constant, but since the damping constants are quite small, they cannot account for the large difference between the theoretical and the measured period. There are two other possible explanations: the system is overdamped, meaning the period increases as time elapses (Taylor 177), or the increase in the average period is related to the increase in fluid viscosity.

A system can only be overdamped if the natural frequency is smaller than the damping constant (Taylor 177). However, even in the 80% glycerin solution, where the damping is the strongest, its damping constant is significantly smaller than its natural frequency, at 0.0318 versus 6.043, confirming that the system is not overdamped.

We then found the period of oscillation between adjacent peaks, troughs, and zeros, and plotted them against elapsed time in Fig. 16 below.

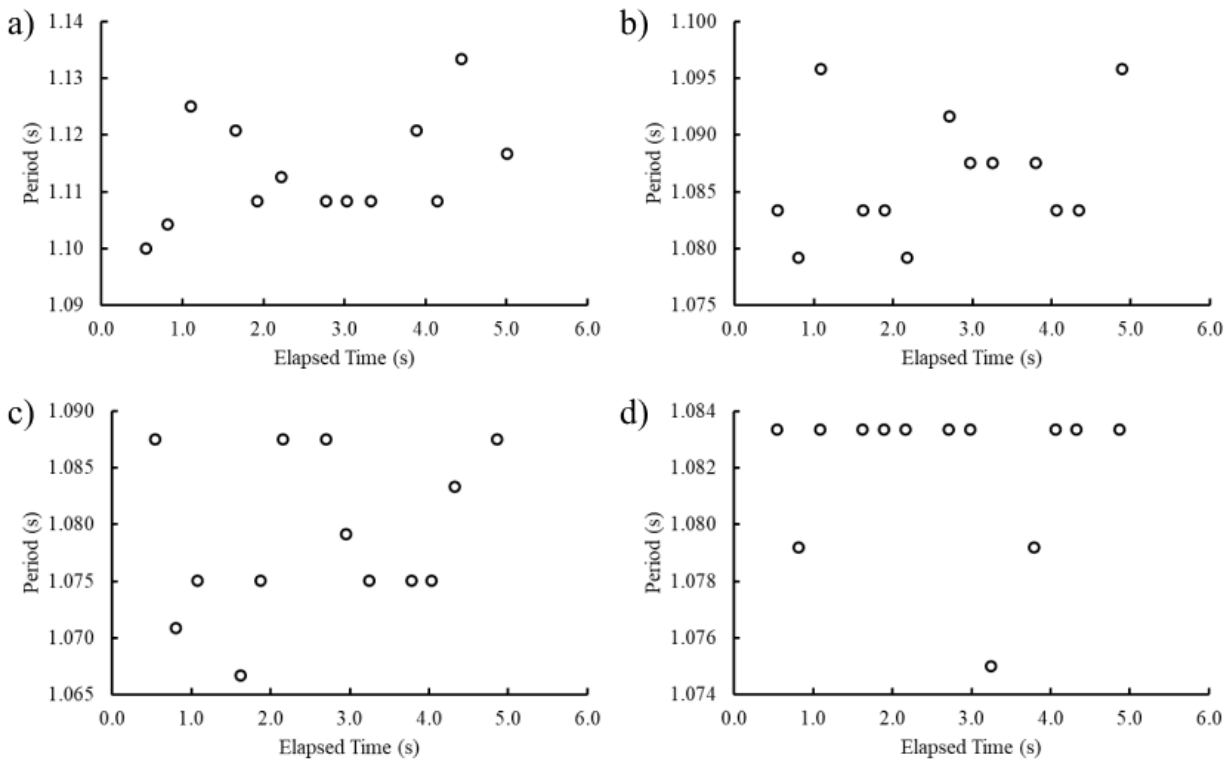

Figure 16: Comparison of the change in the period of oscillation between different concentrations.

Fig. 16a, 16b, and 16c each represent the period when submerged in 80%, 50%, and 20% glycerin respectively. There is no relationship between the period and elapsed time. We also see the period is fluctuating, indicating the system is unlikely to be overdamped. In comparison, Fig. 16d, representing the 0% glycerin, is much more consistent, with just three outliers, suggesting that the presence of glycerin, again, might be an influential factor.

We looked for alternative trends to explain the disagreement. In general, the higher the glycerin concentration, the longer it took the sphere to finish oscillating for 5.75 periods, as shown in Fig. 17 below. This indicates that the change in the average period may be associated with the glycerin concentration.

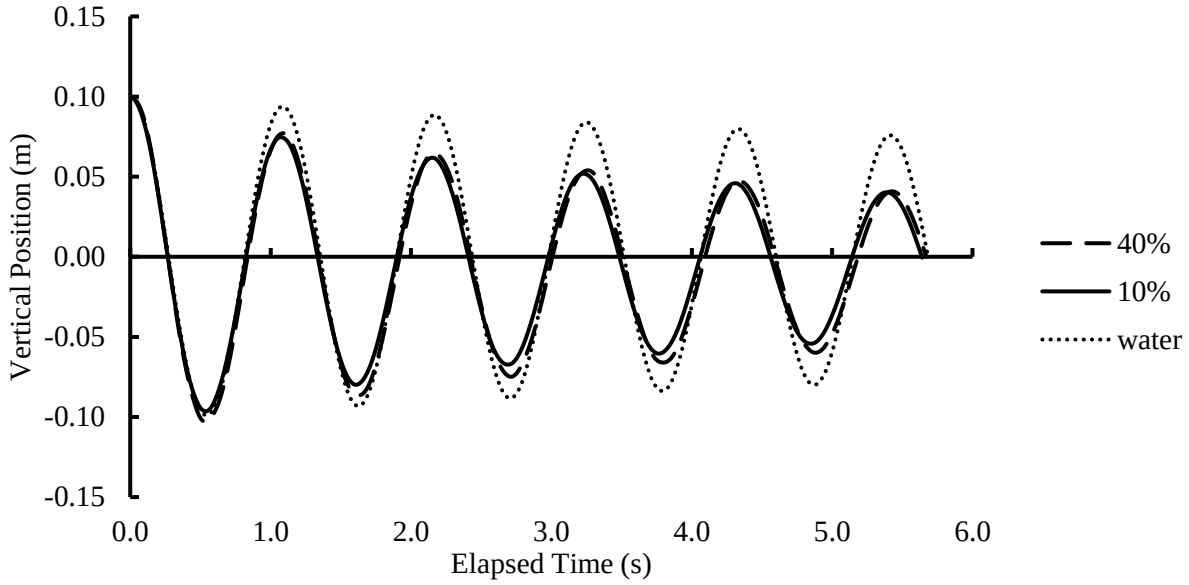

Figure 17: Comparison of measured positions when submerged in 10%, 50%, and 0% glycerin solutions.

We plotted the average period of oscillation against their concentration in Fig. 18 below. As concentration increased, the period of oscillation increased, which suggests the average period is related to glycerin concentration. The line of best fit suggests this relationship is possibly quadratic; however, no clear theoretical evidence supports this relationship.

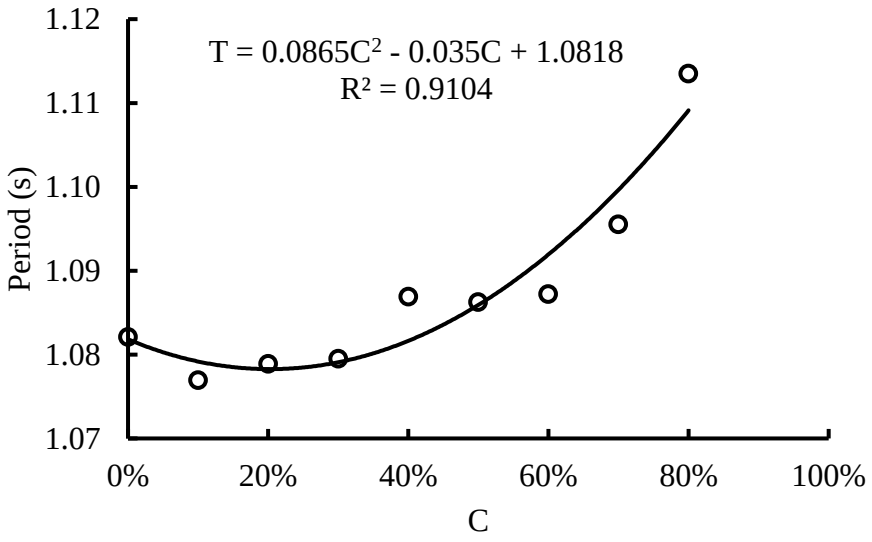

Figure 18: Relationship between the average period of oscillation and glycerin concentrations.

After comparing the theoretical and measured positions, we assessed the limitations of this experiment. The lack of access to pre-calibrated viscometers and the unsuccessful attempt to build and calibrate an accurate capillary viscometer is a source of error. Multiple previous literatures suggested different brands of glycerin might have slightly different physical properties (Segur and Oberstar 2117; “Physical Properties”; Ferreira). Therefore, if the glycerin solutions used in this experiment are thicker than their calculated viscosities, this could partially account for why the theoretical model shows a lightly damped motion, but the measured positions exhibited stronger damping.

The methods used in data processing are another source of error. The random uncertainties of most measurements were lost because they cannot be carried forward after fitting trendlines and interpolating for specific data points using the original measurements. Visually assessing the discrepancies between the theoretical and the measured positions also cannot accurately measure the size of the difference. Therefore, a future improvement could be using techniques that allow the uncertainties to be carried forward and numerically assess the difference between the theoretical and the measured positions.

The most significant limitation of this experiment is that no clear evidence supports the explanations as to why the theoretical and measured positions do not match. Both proposed ideas accounting for the stronger-than-predicted damping effect are only somewhat supported by numerical results. Therefore, potential improvements include measuring the drag coefficient of the system experimentally to incorporate the general drag equation into the theoretical model and studying the physical and chemical properties of glycerin solutions.

Conclusion

The theoretical model disagrees with the measured positions. The main points of disagreements are the stronger-than-predicted damping effects of glycerin solutions and the longer-than-expected periods of oscillation. Multiple ideas as to why they disagree were proposed but verifying them is beyond the scope of this investigation. An alternative model, obtained from manually fitting trendlines lines to the measured positions, was proposed instead. This experiment had many limitations. The most significant one is that there are no explanations for why the theory does not match the measured positions. Some possible improvements include verifying the proposed explanations, obtaining accurate, in situ measurements of glycerin viscosities and investigating the chemical and physical properties of aqueous glycerin solutions.

Works Cited

"2.2.9. Capillary Viscometer Method." *European Pharmacopoeia*, vol. 6, Council of Europe, 2008, pp. 27–28, https://www.uspbpep.com/ep60/2.2.%209.%20capillary%20viscometer%20method%2020209e.pdf. Date of Access: 1 Mar. 2022.

"Calculate Density and Viscosity of Glycerol/Water Mixtures." *University of Reading*, 4 Apr. 2018, https://www.met.reading.ac.uk/~sws04cdw/viscosity_calc.html. Date of Access: 1 June 2022.

Cheng, Nian-Sheng. "Formula for the Viscosity of a Glycerol−Water Mixture." *Industrial & Engineering Chemistry Research*, vol. 47, no. 9, 2008, pp. 3285–3288., doi:10.1021/ie071349z. Date of Access: 1 June 2022.

Ferreira, Abel G.M., et al. "The Viscosity of Glycerol." *The Journal of Chemical Thermodynamics*, vol. 113, Oct. 2017, pp. 162–182., doi:10.1016/j.jct.2017.05.042. Date of Access: 15 July 2022.

Fowler, Michael. "Dropping the Ball (Slowly)." *Stokes' Law*, University of Virginia, https://galileo.phys.virginia.edu/classes/152.mf1i.spring02/Stokes_Law.htm. Date of Access: 1 Mar. 2022.

"Graph Your Oils." *Widman International SRL*, 9 Aug. 2022, https://www.widman.biz/English/Calculators/Graph.html. Date of Access: 1 Aug. 2022.

Mikhailov, M.D., and A.P. Silva Freire. “The Drag Coefficient of a Sphere: An Approximation Using Shanks Transform.” *Powder Technology*, vol. 237, 2013, pp. 432–435., doi:10.1016/j.powtec.2012.12.033. Date of Access: 1 Aug. 2022.

Munson, Bruce Roy, et al. *Fundamentals of Fluid Mechanics*. 7th ed., John Wiley & Sons, Inc., 2013. Date of Access: 1 February 2022.

Physical Properties of Glycerine and Its Solutions. Glycerine Producer's Assoc., 1963, https://aciscience.org/docs/Physical_properties_of_glycerine_and_its_solutions.pdf. Date of Access: 15 July 2022.

Rehm et al. “Flow Drilling: Underbalance Drilling with Liquid Single-Phase Systems.” *Underbalanced Drilling*, Elsevier Science, 2013, pp. 38–108. Date of Access: 15 July 2022.

Taylor, John R. *Classical Mechanics*. University Science Books, 2005, pp. 163–179. Date of Access: 1 Aug. 2022.

Towey, J. J., and L. Dougan. “Structural Examination of the Impact of Glycerol on Water Structure.” *The Journal of Physical Chemistry B*, vol. 116, no. 5, 2011, pp. 1633–1641., doi:10.1021/jp2093862. Date of Access: 15 July 2022.

Troyer, Drew. “Kinematic Viscosity Explained.” *Machinery Lubrication*, Noria Corporation, 2 Dec. 2018, www.machinerylubrication.com/Read/294/absolute-kinematic-viscosity. Date of Access: 1 April 2022.

Tsokos, K. A. *Physics for the IB Diploma*. Cambridge University Press, 2015, pp. 346–347. Date of Access: 1 Feb. 2022.

Urone et al. "12.6: Motion of an Object in a Viscous Fluid." *College Physics*, OpenStax, 2012, pp. 503–505, https://openstax.org/details/books/college-physics. Date of Access: 1 Mar. 2022.

"Viscosity Index." *Anton Paar Wiki*, Anton Paar GmbH, 2022, https://wiki.anton-paar.com/us-en/viscosity-index/. Date of Access: 15 Mar. 2022.

Volk, Andreas, and Christian J. Kähler. "Density Model for Aqueous Glycerol Solutions." *Experiments in Fluids*, vol. 59, no. 5, 2018, doi:10.1007/s00348-018-2527-y. Date of Access: 1 June 2022.

White, Frank M. *Fluid Mechanics*. McGraw-Hill Higher Education, 2016. Date of Access: 15 Jan. 2022.